Minimum latency tracking of rapid variations in two-dimensional storage systems

Minimum-Latency Tracking of Rapid Variations in Two-Dimensional Storage Systems

S. Van Beneden[1], J. Riani[1], J. W. M. Bergmans[1], and A. H. J. Immink[2]

[1]Department of Electrical Engineering, Eindhoven University of Technology, 5600 MB Eindhoven, The Netherlands
[2]Philips Research Laboratories, 5656 AA Eindhoven, The Netherlands

The trend of increasing storage densities results in growing sensitivity of system performance to variations of storage channel parameters. To counteract these variations, more adaptivity is needed in the data receiver. Accurate tracking of rapid variations is limited by latencies in the adaptation loops. These latencies are largely governed by delays of the bit detector. In two-dimensional storage systems, data are packaged in a group of adjacent tracks or rows, and for some of the rows the detection delays can increase dramatically with respect to one-dimensional systems. As a result, the effective latencies in the adaptation loops preclude the tracking of rapid variations and really limit the performance of the system. In this paper, a scheme is proposed that overcomes this problem and that can be used for timing recovery, automatic gain control, and other adaptive circuits. Rapid variations for all the rows are tracked using control information from rows for which detector latency is smallest. This works properly if rapid variations are common across the rows as is the case, for example, for the two-dimensional optical storage (TwoDOS) system. Experimental results for TwoDOS confirm that the scheme yields improved performance with respect to conventional adaptation schemes.

Index Terms—**Adaptation, minimum latency, rapid variations, two-dimensional storage.**

I. Introduction

STEADILY increasing storage densities are a clear trend in storage systems [1]. Reduced margins (e.g., margins with respect to disc tilt, signal-to-noise ratio, SNR) and increased sensitivity to piece-wise and temporal variations of physical storage channel parameters are consequences of this trend and necessitate an increasing amount and an increasing accuracy of adaptivity (e.g., timing recovery, automatic gain control, and other adaptive loops) in the data receiver [2][4]. This accuracy is especially hard to accomplish for the tracking of rapid variations, and is limited by latencies in the adaptation loops.

Another consequence of the increasing densities is that SNRs decrease. As a result, the bit-detector that forms part of the data receiver needs to become more complex to maintain detection reliability. This increased complexity inevitably increases the detection delay. Because this delay contributes to the overall latency in the adaptation loops, it will put an increasingly severe limit on their capabilities to track rapid variations.

A widely adopted solution to improve these tracking capabilities is to base adaptation on tentative decisions with a limited detection delay instead of on final bit decisions [5]. This limited delay enables the adaptation loops to track rapid variations. This solution, however, becomes cumbersome as SNRs decrease, as it becomes more difficult to produce tentative decisions with acceptable reliability and delay.

Besides the increasing density, there is also a general trend of increasing data rates [6]. The development of two-dimensional (2-D) storage systems fits with this trend and permits exploitation of parallelism. The parallelism is achieved by packaging data in a group of adjacent tracks or rows and by parallel processing of these rows. The complexity of 2-D bit detectors increases dramatically with respect to one-dimensional detectors, and also their detection delays can increase dramatically [7], [8].

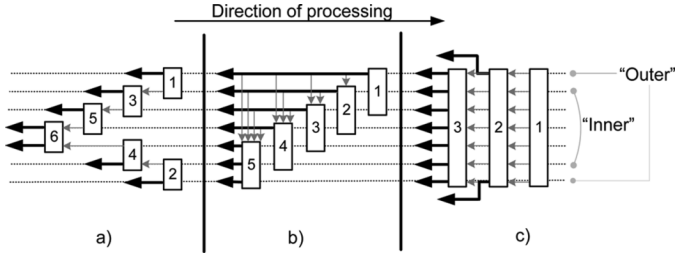

Fig. 1. Examples of 2-D detectors which have varying detection delays for different rows.

In many practical systems, the 2-D detector is split into several smaller units to limit overall complexity [9]–[11]. A couple of schematic models of such detectors reported in literature are shown in Fig. 1. In this figure, seven parallel bit rows are shown: two "outer" rows and five "inner" rows (rows positioned near the center of the group of adjacent rows). The decisions of the different units are indicated in thick black arrows. The different units are numbered in order of execution. If the output of one unit is used as input of a next unit (indicated by the grey arrows), detection delay increases. Different connections between the different units are possible: a) in a "V-shape" [12] (where the two outer rows have the smallest detection delay); b) sequentially starting from the top row [10], [13]; and c) different iterations of the joint detection [7], [8], [14]. In the latter case (different iterations are performed), the decisions of the outer rows will be more reliable than the ones of the inner rows during the first iterations because fewer ISI occurs at the outer rows (due to

Digital Object Identifier 10.1109/TMAG.2006.886844

the 2-D structure, where inner row bits have more neighboring bits than outer row bits) [15]. As a result, decisions of the outer row during an early iteration can be used in the adaptation loops limiting the detection delay of the outer row. For the inner row, however, more iterations are required to achieve an acceptable reliability, resulting in an increased detection delay for the inner rows.

In all these detectors, the detection delay of inner data rows adds substantial latency in the adaptation loops. In the experimental two-dimensional optical storage (TwoDOS) system, for example, the delay for the inner rows is around 100–200 symbol intervals, versus a delay of only 10–20 intervals for the side rows [16], [12]. As a result, the effective latencies in the adaptation loops for these inner rows preclude the tracking of rapid variations and really limit the performance of the system.

Benefiting from the fact that in a 2-D system the delays tend to differ per row, in this paper we propose a scheme that uses control information from rows for which detector latency is smallest to track rapid variations for all the rows. The scheme works efficiently if rapid variations are common across the rows, as is the case, for example, in TwoDOS. In the proposed scheme these rapid common variations are tracked using control information of the rows with the minimum latency in the adaptation loop, while the slow row-dependent variations are tracked using the delayed control information of the specific row under consideration. This scheme can be used for timing recovery, automatic gain control (AGC), and other adaptation loops, and is analyzed and validated experimentally. It shows improved performance with respect to conventional adaptation loops in case substantial loop-delays are present.

The scheme that is proposed in this paper is general and can be applied to any 2-D storage system. In this paper a particular example of a 2-D storage system, namely the TwoDOS system, is used to illustrate the design of the adaptation loops and to provide experimental results. In Section II, a general receiver model for 2-D storage systems is discussed and a general parameter-domain model of an adaptation loop is derived from this receiver model. The effect of latencies on the performance of adaptation loops is discussed in Section III. The general scheme for minimum-latency tracking of rapid variations is explained in Section IV. In Section V the design of first-order loops according to the described scheme is explained, analyzed and verified by means of simulations. These first-order loops can be used, for example, for dc compensation and AGC. Minimum-latency tracking suited for timing recovery is the subject of Section VI, where the design of second-order loops is discussed. Finally Section VII presents experimental results for the TwoDOS system. These results show that the new scheme improves the performance of the system with respect to conventional schemes.

II. Receiver Model

A data receiver model for 2-D storage systems is shown in Fig. 2. Inputs of the model are N_R digitized replay signals, where N_R is the number of adjacent data rows. In magnetic recording, for example, these replay signals are generated by read heads. The data receiver contains a bit detector that relies upon a well-defined relationship between the stored data and the desired detector input signals [5]. This relationship is often characterized by a so-called target response, and is often linear. To approach this relationship as closely as possible, the replay signals are preprocessed by digital signal processing blocks (e.g., timing adjustment, prefilter, dc compensation) before they enter the detector. Because physical parameters of the storage channel (e.g., bandwidth, amplitude, dc offset, etc.) may vary in time, adaptivity is needed to counteract the parameter variations such that the relationship between the stored data and the detector input signal does not vary in time and is consistent with the target response. To this end the receiver includes a preprocessing block with several adjustable parameters (e.g., an AGC gain, equalizer taps, etc.) that are controlled by dedicated adaptation loops.

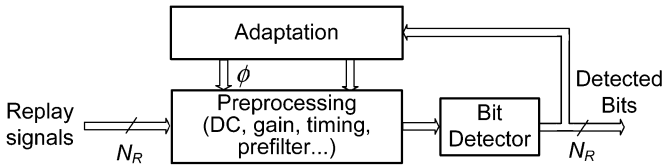

Fig. 2. Data receiver model for 2-D storage system.

For each adjustable parameter, a value ϕ is produced by the adaptation block and is subsequently used in the preprocessing blocks to counteract system parameter variations. We denote the ideal value of the adjustable parameter by θ (clearly θ depends on the channel parameters and can hence be time-varying). Ideally ϕ should be equal to to θ. A difference Δ between ϕ and θ results in an undesired mismatch between the actual and the desired detector input signal. Accurate tracking of θ (or equivalently, minimizing Δ) will minimize this mismatch and as result will improve receiver performance. An example of an adaptive parameter is the dc-offset for a specific row. The value ϕ is the estimated dc-offset while θ is the ideal dc-offset, i.e., the (possibly time-varying) dc-offset that has to be added to the incoming signal to eliminate any residual dc-offset in the detector input.

The preprocessing block, the bit detector and the adaptation block form a closed loop which comprises the individual adaptation loops. These loops are of the data-aided (DA) type. A DA adaptation loop uses the detected bits as side information to facilitate adaptation. As a result the bit detector forms part of the loop and the detection delays introduce a latency in the loop. This latency will limit the capability of the loop to track fast variations of θ. The effect of latency on the tracking capabilities of an adaptation loop is subject of the next section.

III. Effect of Latency on Loop Behavior

In the left part of Fig. 3, a discrete-time parameter-domain model of an adaptation loop with latency is given [17]. This model is valid in the tracking mode of operation. An ideal parameter value θ is the first input of the model and this value can be time-varying (the time index k is omitted in the remainder of this paper for notational simplicity). A noise component ν (input-referred noise) is the second input of the loop. The purpose of the loop is to minimize the mismatch Δ between the

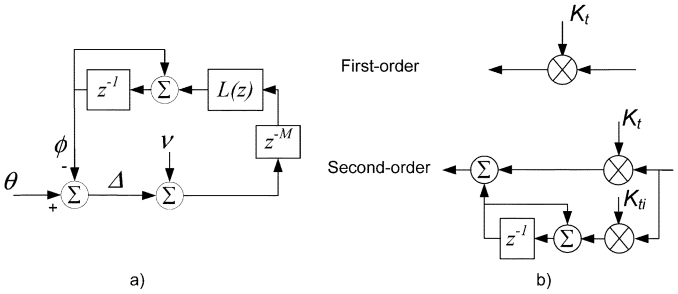

Fig. 3. (a) General parameter-domain model of an adaptation loop with a loop filter characterized by the transfer function $L(z)$. This loop is sampled at the baud rate $1/T$, i.e., z^{-1} corresponds to a delay of T seconds. b) Loop filters of first-order adaptation loop and of second-order high-gain adaptation loop.

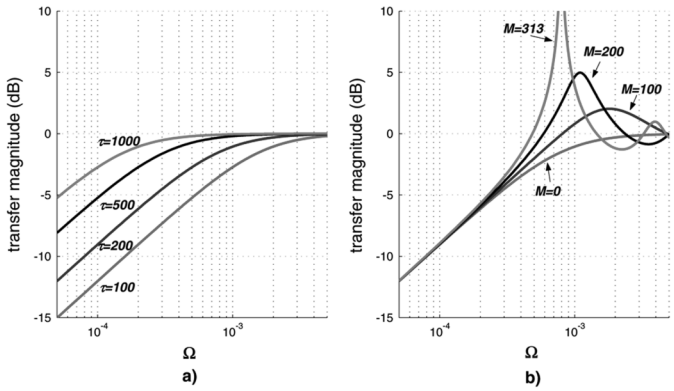

Fig. 4. Mismatch transfer magnitudes of a first-order adaptation loop as function of the normalized frequency $\Omega = \omega T/(2\pi)$. a) No loop-delay, $M = 0$ (left part). b) Time constant $\tau = 200$ (right part).

ideal parameter value θ and its estimate ϕ. To generate this estimate ϕ, a loop filter with transfer characteristic $L(z)$ followed by an ideal integrator is used. In the right part of Fig. 3 different types of loop filters are shown. In most cases (e.g., for dc control, automatic gain control, adaptive equalization) a first-order loop is sufficient. In this case, the loop filter is just a multiplier: $L(z) = K_t$, where K_t is the total gain of the loop. Timing recovery, however, requires a second-order adaptation loop in order to be able to track frequency variations. To this end, the loop filter needs to be extended with an ideal integrator and a second gain K_{ti}, which determines together with K_t the behavior of the loop.

In the model, a delay of M symbol intervals is present which mimics the overall latency in the loop. The model has a low-pass frequency characteristic. If θ changes, then ϕ will track the slow variations but not the fast ones. In this way also the high-frequency noise components ν are rejected.

A. Loop Behavior

As the dynamic properties of the loop do not depend on the input-referred noise ν, we neglect this noise for the time being. The adaptation loop is linear and can be characterized by means of the parameter transfer function $G_\phi(z) = \Phi(z)/\Theta(z)$ and the mismatch transfer function $G_\Delta(z) = \Delta(z)/\Theta(z)$ (the response in the z-domain of respectively ϕ and Δ to the loop excitation θ). Only first-order adaptation loops are considered here. Extension to second-order loops is straightforward. For first-order loops the loop filter has transfer function $L(z) = K_t$, where K_t is the total gain of the loop. The mismatch transfer function $G_\Delta(z)$ is evaluated to be

$$G_\Delta(z) = \frac{z^M(z-1)}{z^M(z-1)+K_t}. \tag{1}$$

Let θ be a unit step function. Then, for $M = 0$, the mismatch can be approximated as an exponentially decaying function $e^{-k/\tau}$, where τ is the time constant of the loop expressed in sampling intervals. For small K_t, the time constant can be expressed as $\tau \approx 1/K_t$.

The mismatch magnitude responses for varying time constants τ and loop-delays M are shown in Fig. 4. In the left part of the figure, the response is shown for varying time constants τ and zero delay ($M = 0$). By increasing τ, the equivalent bandwidth of the loop decreases. The equivalent bandwidth is defined by the normalized loop cutoff frequency $\Omega_c = K_t/2\pi$, i.e., the normalized frequency where the amplitude of the transfer function is -3 dB. In the right part of Fig. 4, the magnitude response of the mismatch transfer function is shown for a given time constant $\tau = 200$ and for varying loop-delays M. An increasing resonance peak appears near the cutoff frequency Ω_c for increasing loop-delays. If the ideal parameter value θ has spectral content in this frequency region, the total mismatch power will increase due to this resonance peak (in other words, the loop enhances rather than suppresses variations around this frequency).

If the delay is increased too much, the loop can become unstable. The edge of the stability region demarcates a relationship between the loop-delay and the time constant of the loop: $\tau \simeq (2M+1)/\pi$ [18]. This relationship reveals the smallest allowable time constant for a given loop-delay.

The responses shown in Fig. 4 indicate that in a practical system the presence of a large loop-delay can influence the choice of a proper time constant considerably. In general, to limit resonance effects or even to avoid instability, a larger time constant with respect to the zero loop-delay case is needed, which will make the loop less capable of tracking fast parameter variations.

B. Gradient Noise

Gradient noise is defined as the additional mismatch in the adaptation loop due to the input-referred noise ν. This gradient noise does not introduce a bias in the estimate ϕ but influences the variance of the mismatch Δ:

$$\sigma_\Delta^2 = \frac{T}{2\pi}\int_{-\frac{\pi}{T}}^{\frac{\pi}{T}} P_\nu(e^{j\omega T})|G_\phi(e^{j\omega T})|^2 d\omega, \tag{2}$$

where $P_\nu(e^{j\omega T})$ is the power spectral density of ν. If ν is assumed to be white and Gaussian, then the mismatch variance can be expressed as $\sigma_\Delta^2 = \sigma_\nu^2 B_l$, where $B_l = (K_t/2 - K_t)$ is the normalized equivalent noise bandwidth (if the loop-delay M is omitted, otherwise the noise bandwidth B_l will be slightly higher due to the resonance effect) and σ_ν^2 is the variance of the input-referred noise ν. In practice, K_t is much smaller than

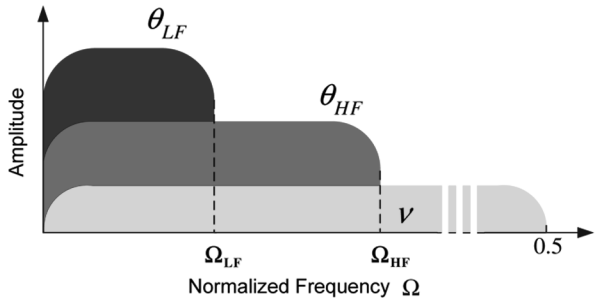

Fig. 5. Spectral content of different inputs of a control loop. The input parameter value θ is assumed to consist of two components: θ_{LF} and θ_{HF}. Furthermore the spectrum of the noise ν is also shown.

unity, hence $B_l \simeq K_t/2$. The variance of Δ can then be expressed as

$$\sigma_\Delta^2 \simeq \frac{K_t \sigma_\nu^2}{2}. \tag{3}$$

From this equation, it is clear that σ_Δ^2 is proportional to K_t, which means that the mismatch variance will increase for decreasing time constants.

IV. Minimum-Latency Adaptation

In a 2-D storage system, the detection delay can be especially large for the inner rows. This large delay results in a large latency in the adaptation loops for these rows. As described in Section III, this latency makes the loops incapable of tracking rapid parameter variations. In a 2-D system like the TwoDOS system, it is possible to use control information from bit rows with smaller latencies to counteract these rapid variations. The principle of using control information with the smallest latency is referred to as the minimum-latency adaptation strategy. As a consequence, the aim is to design adaptation loops that make use of the minimum-latency control information to counteract rapid variations in all rows.

The minimum-latency adaptation strategy is only applicable if rapid variations of system parameters are common for all the rows. Subject to this basic premise, the overall model of the ideal parameter value θ should be: $\theta = \theta_{\mathrm{LF}} + \theta_{\mathrm{HF}}$, where θ_{LF} is a slowly varying, row-dependent component (with highest frequency Ω_{LF}) and θ_{HF} is a rapidly varying component which is common for all the rows (highest frequency Ω_{HF} and $\Omega_{\mathrm{HF}} > \Omega_{\mathrm{LF}}$). The parameters of all rows must show this behavior: possibly different low-frequency content but the same high-frequency content. The spectral content of the ideal parameter value θ together with the input referred noise ν (assumed to be Gaussian and white) is sketched in Fig. 5.

The basic premise that rapid variations are common across the rows can be validated experimentally for the TwoDOS system. By way of illustration we consider the dc control loops [19], which serve to counteract time-varying dc-offsets in the rows. Here, dc-offset estimates ϕ_O for every row are generated by separate adaptation loops where the gain values K_t are chosen such that ϕ_O is able to track fast variations of the ideal dc-offset values θ_O (in the experimental estimates $K_t = 0.06$ was found to be a proper value). Because $G_\phi(z)$ has unit amplitude up to the normalized loop cutoff frequency ($\Omega_c \approx 0.01$), the spectral content of ϕ_O resembles the spectral content of θ_O up to Ω_c (if noise is neglected). The spectral content of the inner-row dc-offset estimate ϕ_O is shown in Fig. 6. This estimate ϕ_O is composed of different components which are also shown in the figure. The common dc-offset component ϕ_{Oc} is calculated by averaging the dc-offsets over all rows. The row-dependent dc-offset component ϕ_{Or} is obtained by subtracting ϕ_{Oc} from ϕ_O. Finally, the power spectral density P_ν of the input-referred noise ν is obtained by taking the Fourier transform of the difference between the ideal and the actual detector input. For low frequencies, the row-dependent component ϕ_{Or} is the most important component of ϕ_O. At higher frequencies ($\Omega = [7e^{-4}, 2e^{-3}]$), the common component ϕ_{Oc} determines ϕ_O. For even higher frequencies the offset estimate is determined by the input-referred noise ν. The common offset component ϕ_{Oc} can be explained by the fact that certain channel parameters (e.g., the amount of defocus and the cover layer thickness) are common across the adjacent rows. For the TwoDOS system, the cover layer thickness exhibits variations that extend over a limited amount of bits (100–1000 bits). As a result these variations result in high-frequency common offset variations. Other reasons for fast common channel parameter variations are: dust, fingerprints, scratches on the disc, dropouts, etc. [20], [22]. These observations lend support to the assumed parameter model, not just for TwoDOS but also for other 2-D storage systems.

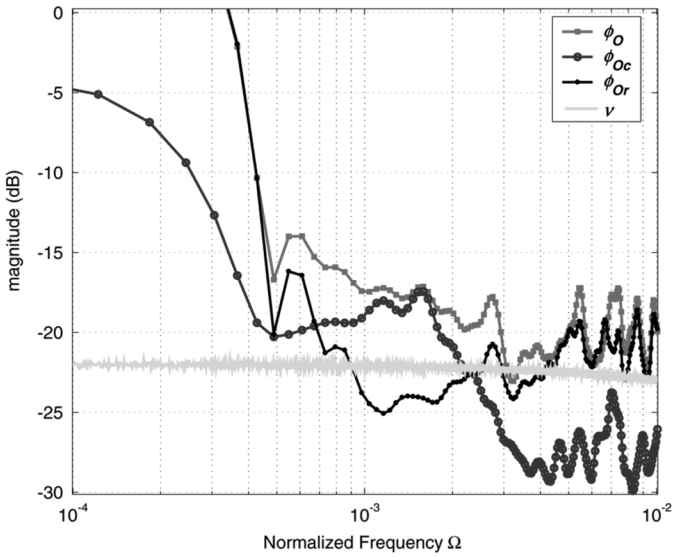

Fig. 6. Experimentally estimated spectral content of dc-offsets in TwoDOS system: the dc-offset estimate ϕ_O of the inner row and its different components: ϕ_{Oc} and ϕ_{Or}. Also, the spectrum P_ν of the input noise ν is shown.

A basic assumption of the minimum-latency adaptation strategy is that the common parameter value θ_{HF} is tracked using the minimum-latency control information. In reality, also small and relatively slow variations occur between the rows. In the minimum-latency adaptation strategy these slow row-dependent components θ_{LF} are handled by using delayed information from the inner rows.

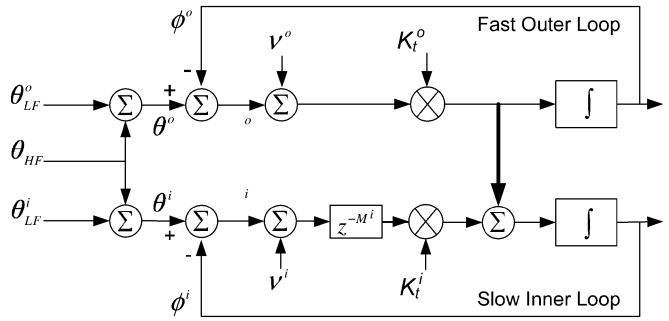

Fig. 7. Parameter-domain model of the first-order minimum-latency adaptation loops.

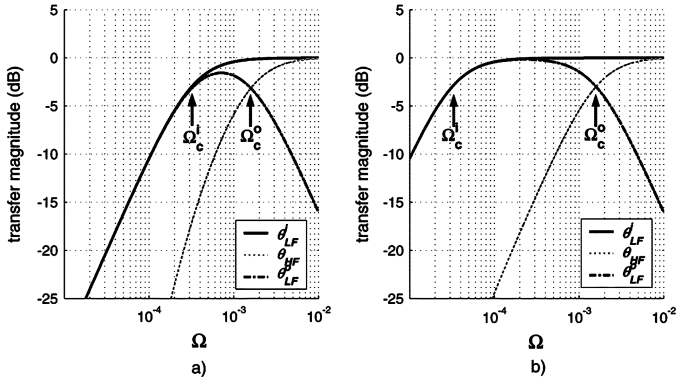

Fig. 8. Mismatch transfer magnitudes of the inner minimum-latency adaptation loop as a function of the normalized frequency $\Omega = \omega T/(2\pi)$. The outer loop has a time constant $\tau^o = 100$ bits. The inner loop has the following time constants: (a) $\tau^i = 5\tau^o$ (left figure). (b) $\tau^i = 50\tau^o$ (right figure).

In Section V, the minimum-latency adaptation strategy for first-order loops is proposed and analyzed (applicable to the AGC loop and the dc control loop). The minimum-latency strategy is applied to second-order loops (as used for timing recovery) in Section VI. In Section VII, the experimental validation of the minimum-latency adaptation strategy is presented for the TwoDOS system.

V. First-Order Minimum-Latency Adaptation Loops

To illustrate the application of the minimum-latency strategy to first-order loops, only two rows (instead of N_R rows) are considered for simplicity: an "outer" row with small latency and an "inner" row with large latency. Furthermore, every row has a separate adaptation loop. In Fig. 7, a parameter-domain model of the minimum-latency first-order adaptation loops is shown together with the assumed parameter model.[1] The input-referred noises ν^i and ν^o are inputs of the model and are uncorrelated. Furthermore, a delay of M^i bits is present in the inner loop to mimic the large detection delay of the inner row. In reality, also a small detection delay $(M^o < M^i)$ is present in the outer loop, but this delay is omitted in the model to simplify the analysis. This relatively small delay will not have a major influence on the overall loop behavior. Following the minimum-latency adaptation strategy, the outer loop is dimensioned to be fast (large loop gain K_t^o) and the inner loop is dimensioned to be slow (small loop gain K_t^i).

The key innovative feature of the minimum-latency adaptation strategy is the connection between the fast outer loop and the slow inner loop. This connection (thick line in Fig. 7) provides the inner loop with control information concerning the fast common parameter θ_{HF} that is not yet available in the inner loop due to the delay M^i. As a result, ϕ^i is able to track fast variations of θ_{HF} (using control information of the outer row) and slow variations of θ_{LF}^i (using delayed control information of the inner row). However, due to the connection a portion of θ_{LF}^o will inevitably be present in the estimate ϕ^i. In Section V-A, the basic loop behavior is analyzed which will prove that this portion is sufficiently small.

[1]In the TwoDOS system, there are two outer rows that can be used to derive the common rapid variations from. The outputs of these outer loops are averaged and the result is used in the inner rows. This procedure fully exploits all minimum-latency information.

A. Basic Behavior

Because the inner loop is dimensioned to be slow, the delay M^i of the inner loop will not have strong impact on the loop behavior (see Section III-A). For this reason we initially omit delay in our analysis of the basic behavior, i.e., we set $M^i = 0$. As the dynamic properties of the loops do not depend on the input noises ν^i and ν^o, these input noises are neglected. By transformation into the z-domain, the basic loop behavior can be analyzed. The inner loop will not show first-order behavior anymore but becomes essentially a second-order adaptation loop, whose behavior is determined by the total gains K_t^i and K_t^o. The z-transform of the inner-row estimate ϕ^i can easily be derived to be

$$\begin{aligned}\Phi^i(z) &= \frac{K_t^i}{z-1+K_t^i}\Theta_{\mathrm{LF}}^i(z) \\ &\quad + \left(\frac{K_t^i}{z-1+K_t^i} - \frac{K_t^o(z-1)}{(z-1+K_t^o)\left(z-1+K_t^i\right)}\right)\Theta_{\mathrm{HF}}(z) \\ &\quad - \frac{K_t^o(z-1)}{(z-1+K_t^o)\left(z-1+K_t^i\right)}\Theta_{\mathrm{LF}}^o(z) \end{aligned} \tag{4}$$

where $\Phi^i(z)$, $\Theta_{\mathrm{LF}}^i(z)$, $\Theta_{\mathrm{LF}}^o(z)$, and $\Theta_{\mathrm{HF}}(z)$ are the z-transform of respectively ϕ^i, θ_{LF}^i, θ_{LF}^o, and θ_{HF}.

From (4), it is clear that the estimate ϕ^i of the ideal parameter value θ^i is determined by all three ideal parameter components: θ_{LF}^i, θ_{HF}, and θ_{LF}^o. In Fig. 8, the mismatch magnitudes due to these components are plotted for two different inner-row time constants τ^i while fixing the outer-loop time constant τ^o at 100 bits. In the left part of the figure, the magnitudes are shown for the case the inner-row adaptation loop is 5 times slower than the outer-row adaptation loop, i.e., $\tau^i = 5\tau^o$. In the right part of the figure $\tau^i = 50\tau^o$. The mismatch magnitudes $|\Delta^i(z)| = |\Theta^i(z) - \Phi^i(z)|$ due to each component are discussed.

- θ_{LF}^i: all spectral content of θ^i (and as a result also of θ_{LF}^i) up to the inner-loop cutoff frequency $(\Omega_c^i = K_t^i/2\pi)$ is present in the estimate ϕ^i and is not present in the mismatch Δ^i. As a consequence the inner loop should be designed such that $\Omega_c^i \geq \Omega_{\mathrm{LF}}$.

- $\theta_{\rm HF}$: this is the high-frequency component of θ^i and is present in the estimate ϕ^i up to the cutoff frequency of the outer loop ($\Omega_c^o = K_t^o/2\pi$). The key objective of the minimum-latency adaptation strategy is hereby achieved: $\theta_{\rm HF}$ is present in the estimate ϕ^i up to the outer-loop cutoff frequency Ω_c^o despite the fact that the inner adaptation loop has a cutoff frequency $\Omega_c^i < \Omega_c^o$. The time constant τ^o should be chosen such that: $\Omega_c^o \geq \Omega_{\rm HF}$.
- $\theta_{\rm LF}^o$: the outer-loop low-frequency component $\theta_{\rm LF}^o$ should be rejected as much as possible. This is accomplished if the inner loop is designed properly: $\Omega_c^i > \Omega_{\rm LF}$.

As a conclusion the following criteria for the proper choice of the loop time constants are formulated:

$$\text{Outer loop: } \tau^o \leq \frac{1}{2\pi\Omega_{\rm HF}};$$
$$\text{Inner loop: } \tau^i \leq \frac{1}{2\pi\Omega_{\rm LF}}. \quad (5)$$

B. Gradient Noise

The outer-loop gradient noise is not influenced by the inner-loop noise ν^i and has the same variance as expressed in (2). But as expected, the total amount of gradient noise in the inner loop has an extra component due to the minimum-latency adaptation strategy. The variance of the inner-loop mismatch Δ^i is evaluated to be

$$\sigma_{\Delta^i}^2 = \frac{T}{2\pi}\int_{-\frac{\pi}{T}}^{\frac{\pi}{T}} P_{\nu^i}(e^{j\omega T})|G_{\phi^i}(e^{j\omega T})|^2 d\omega + \frac{T}{2\pi}\int_{-\frac{\pi}{T}}^{\frac{\pi}{T}} P_{\nu^o}(e^{j\omega T})|G_{\phi^o}(e^{j\omega T})|^2 d\omega \quad (6)$$

where $P_{\nu^i}(e^{j\omega T})$ and $P_{\nu^o}(e^{j\omega T})$ are the power spectral densities of respectively ν^i and ν^o. The input-referred noise ν^o of the outer loop leaks into the inner loop according to the open-loop transfer function $G_{\phi^o}(z) = \Phi^o(z)/\Theta^o(z)$ which has a bandwidth $B_l = K_t^o/2$ (under the assumption $K_t^i < K_t^o \ll 1$ and $M^i = 0$). In case the input noises ν^i and ν^o are assumed to be white and Gaussian, the variance of the inner-loop mismatch Δ^i can be approximated as

$$\sigma_{\Delta^i}^2 \simeq \frac{K_t^i \sigma_{\nu^i}^2}{2} + \frac{K_t^o \sigma_{\nu^o}^2}{2} \quad (7)$$

where $\sigma_{\nu^i}^2$ and $\sigma_{\nu^o}^2$ are the variances of the input noises ν^i and ν^o, respectively. From this equation, it is clear that the gradient noise in the inner loop is proportional to K_t^i and K_t^o, and dominated by the outer-loop noise ν^o (because $K_t^o > K_t^i$). Therefore the variances of the inner- and outer-loop mismatches are approximately equal.

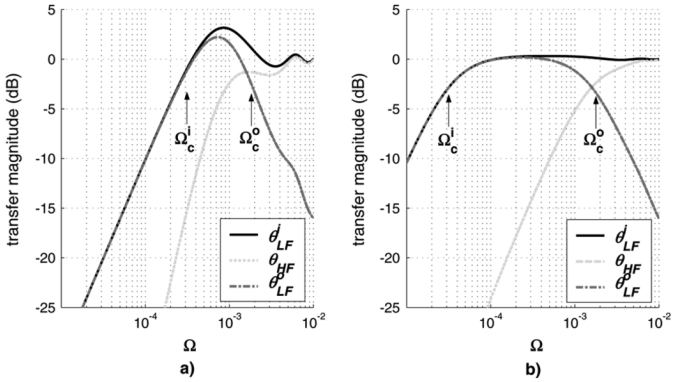

Fig. 9. Mismatch transfer magnitudes of the inner minimum-latency adaptation loop (first-order) as a function of the normalized frequency $\Omega = \omega T/(2\pi)$. The inner loop has a delay of $M^i = 200$ bits. The outer-loop time constant τ^o is equal to 100 bits. The inner loop has the following time constants: (a) $\tau^i = 5\tau^o$ (left figure). (b) $\tau^i = 50\tau^o$ (right figure).

C. Behavior of the Inner Loop With Latency

The insertion of a delay of M^i bit intervals changes the behavior of the inner adaptation loop. The z-transform of the inner-loop mismatch Δ^i is evaluated to be

$$\Delta^i(z) = \frac{z-1}{z-1+z^{-M^i}K_t^i}\Theta_{\rm LF}^i(z) + \left(\frac{z-1}{z-1+z^{-M^i}K_t^i} - \frac{K_t^o(z-1)}{(z-1+K_t^o)\left(z-1+z^{-M^i}K_t^i\right)}\right)\Theta_{\rm HF}(z) - \frac{K_t^o(z-1)}{(z-1+K_t^o)\left(z-1+z^{-M^i}K_t^i\right)}\Theta_{\rm LF}^o(z). \quad (8)$$

The corresponding transfer magnitudes are shown in Fig. 9 for the following conditions: $M^i = 200$ bits and $\tau^o = 100$ bits. The inner adaptation loop is dimensioned to be slow: $\tau^i = 5\tau^o$ in the left part of the figure and $\tau^i = 50\tau^o$ in the right part of the figure. The effect of the insertion of a delay in the inner loop can be evaluated by comparing Fig. 9 with Fig. 8. Especially the left plot is substantially changed with respect to the situation without delay: a resonance effect clearly appears in the transfer magnitudes at frequencies in the vicinity of the cutoff frequency Ω_c^i of the slow inner loop. Consequently, if the second design criterium ($\Omega_c^i \geq \Omega_{\rm LF}$) is obeyed, the correct estimation of the slow parameter variations $\theta_{\rm LF}^i$ is guaranteed and also the outer-row parameter $\theta_{\rm LF}^o$ is rejected sufficiently in the inner-row estimate ϕ^i. The estimation of the high-frequency component $\theta_{\rm HF}$ will deteriorate slightly as the mismatch magnitude is slightly increased near the cutoff frequency Ω_c^o of the outer-row adaptation loop. Consequently if also the first design criterium ($\Omega_c^o \geq \Omega_{\rm HF}$) is obeyed, the tracking capabilities of the minimum-latency adaptation loops with and without a loop-delay will be comparable. The transfer magnitude of a slow inner loop (right part of the figure) is not (or just slightly) influenced by the insertion of the delay. This behavior is expected based on the analysis of Section III-A.

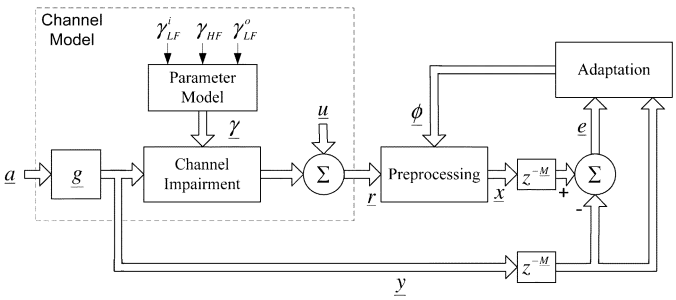

Fig. 10. Simulation model.

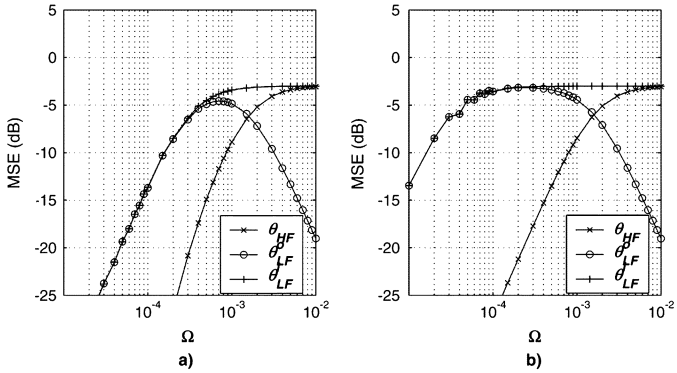

Fig. 11. MSE of the inner row vs. the normalized frequency Ω of the different dc-offset components. The following settings are used: $M^i = 0$, $\tau^o = 100$ bits, $\tau^i = 500$ [left plot a)] and $\tau^i = 5000$ bits [right plot b)].

D. Simulation Results

Simulation results were obtained by simulating the model presented in Fig. 10. Replay signals $\underline{r}$ are produced by passing the data bits $\underline{a}$ (where $\underline{a} = [a_1[k] \dots a_{N_R}[k]]$) to a simple channel model that has three basic parts. First, ideal detector input signals $\underline{y}$ are generated by convolving $\underline{a}$ with fixed 2-D target responses $\underline{g}$ (where $\underline{g} = [g_1 \dots g_{N_R}]$). The second part of the channel model is a channel impairment block which corrupts $\underline{y}$ according to time-varying system parameter values $\underline{\gamma} = [\gamma_1 \dots \gamma_{N_R}]$. In this section dc-offsets are considered as channel impairments, i.e., $\underline{\gamma}$ are the dc-offsets induced by the channel. Only one outer-row value ($\gamma^o = \gamma_1$) and one inner-row value ($\gamma^i = \gamma_{(N_R-1)/2}$) are nonzero and they are both generated according to the parameter model of Fig. 7: $\gamma^o = \gamma^o_{\rm LF} + \gamma_{\rm HF}$ and $\gamma^i = \gamma^i_{\rm LF} + \gamma_{\rm HF}$, where $\gamma^o_{\rm LF}$ and $\gamma^i_{\rm LF}$ are slowly varying components and $\gamma_{\rm HF}$ is a rapidly varying component. To simplify the simulation only sinusoidally time-varying components are considered, i.e., the dc-offsets induced by the channel vary slowly as a sinusoidal function of time. Moreover, only one component has an amplitude equal to one while the other components all have zero amplitude, i.e., the responses to individual parameter components are simulated and not to a combination of different parameter components. Finally, white Gaussian noise components $\underline{u}$ are added to the channel impairment output signals to produce the replay signals $\underline{r}$. The noise components of the different rows are uncorrelated and have the same variance.

These replay signals $\underline{r}$ are input of a preprocessing block that tries to undo the corruption induced by the channel impairment block. For this reason, this preprocessing block utilizes estimates $\underline{\phi}$ of the ideal values $\underline{\theta}$ (for dc-offsets $\underline{\theta} = -\underline{\gamma}$). To mimic detection delays, the outputs $\underline{x}$ of the preprocessing block are delayed with delays $\underline{M} = [M^1 \dots M^{N_R}]$. To simplify the simulation, the delay of the outer rows is chosen to be 0 ($M^1 = M^o = 0$) and the delay of the inner rows is set to M^i bits. Error signals $\underline{e}$ are calculated by subtracting delayed versions (with delays $\underline{M}$) of $\underline{y}$ from these delayed versions of $\underline{x}$. Finally, an adaptation block uses $\underline{e}$ and delayed versions of $\underline{y}$ to produce estimates $\underline{\phi}$ which are used by the preprocessing block. The adaptation block utilizes the ZF technique [17] to produce the estimates. The variances of the input-referred noises are similar ($\sigma^2_{\nu^i} \approx \sigma^2_{\nu^o}$) provided that the variances of the noise components are similar ($\sigma^2_{u^i} \approx \sigma^2_{u^o}$), which is the case in our simulations.

The SNR of the system is defined as

$$\mathrm{SNR} = \frac{\sum g_k^2}{\sigma^2_{u^i}} = \frac{\sum g_k^2}{\sigma^2_{u^o}}. \tag{9}$$

The mean square error (MSE) of the inner row is defined as

$$\mathrm{MSE}_i = \mathrm{E}[e_i^2] \tag{10}$$

where e_i is the error of the inner row. Because MSE quantifies the mismatch between the actual and the desired detector input, it is closely related to bit error rate. As a result, it is a good measure to quantify the performance of the adaptation loops.

The MSE of the inner row is plotted in Fig. 11 as a function of the normalized frequency Ω of the different ideal dc-offset components $\theta^i_{\rm LF}$, $\theta_{\rm HF}$, and $\theta^o_{\rm LF}$ (only one parameter is nonzero at a time). Because the dc-offset estimates $\underline{\phi}$ are added to $\underline{r}$ in the preprocessing block, any dc-offset mismatch is part of the error $\underline{e}$. As a result, the MSE plotted in Fig. 11 is directly related to the mismatch transfer magnitudes shown in Fig. 8. The time constant τ^o of the outer loop is 100 bits ($\tau^o = 100$ bits), while the time constant τ^i of the inner control loop is 500 bits for the left plot ($\tau^i = 500$ bits) and 5000 bits for the right plot ($\tau^i = 5000$ bits). These simulation results exactly match the theoretical results derived in the previous section.

A validation of the minimum-latency adaptation strategy is shown in Fig. 12: a comparison between delayed individual adaptation loops and delayed minimum-latency adaptation loops. The gain in inner-row minimum MSE (MMSE) is shown as function of the loop-delay M^i for two different SNR values. Here, MMSE is defined as the minimum MSE obtained by tuning the time constants τ^i and τ^o. In this simulation, sinusoidal dc-offset variations (with unit amplitude) are considered with the following frequencies: $\Omega^i_{O,\rm LF} = \Omega^o_{O,\rm LF} = 10^{-5}$ and $\Omega_{O,HF} = 10^{-4}$. The conditions are representative for severe but not extreme situations (scratches, dropouts, fingerprints...) in an experimental system [20]. Due to the resonance effect, the insertion of a delay into the inner loop causes a substantial degradation in MMSE for the individual adaptation loops (which is in agreement with the analysis of Section III-A).

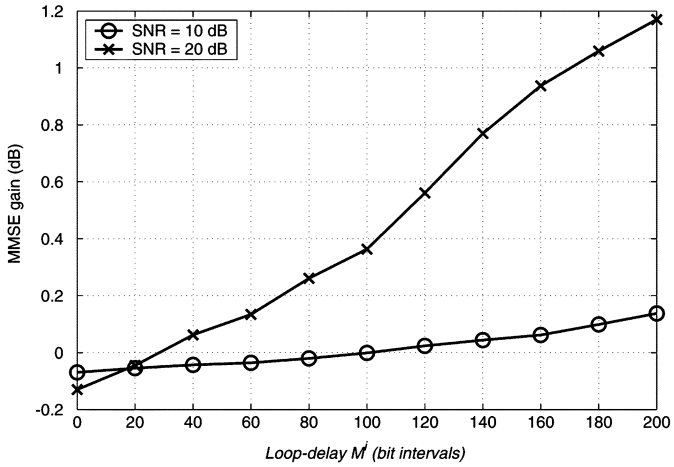

Fig. 12. Gain in MMSE of the minimum-latency adaptation loops with respect to the individual adaptation loops. The gain in MMSE of the inner row is plotted as a function of the inner-row loop-delay M^i for two different SNR values: 10 and 20 dB.

The minimum-latency adaptation strategy however guarantees the tracking of rapid common offset variations $\theta_{O,\mathrm{HF}}$ and as a consequence the MMSE degrades less than for individual adaptation if loop-delays are large. In general, for small loop-delays the minimum-latency adaptation loops perform worse because outer row noise ν^o leaks into the inner-loop mismatch Δ_O^i and at the same time the tracking capabilities of the individual and the minimum-latency loops are comparable. For larger loop-delays, the minimum-latency adaptation loops outperform the individual adaptation loops because of the strongly improved tracking of rapid common variations θ_{HF}. For low SNR values (in the figure for $\mathrm{SNR} = 10$ dB), the choice of the optimal time constants is mainly dominated by the avoidance of gradient noise and not by the minimization of the mismatch error due to fast parameter variations. For this reason, the MMSE for the individual and the minimum-latency adaptation loops will not differ much. For delays larger than 100 bits the minimum-latency adaptation loops outperform the individual loops, even though the MMSE gain is small (0.2 dB for $M^i = 200$ bits). For high SNR values ($\mathrm{SNR} = 20$ dB), the gain in MMSE by using the minimum-latency adaptation loops increases. The time constants can be primarily tuned to improve the tracking capabilities and not to limit the amount of gradient noise in the loop. For a large loop-delay $M^i = 200$ bits, the gain in MMSE accumulates up to 1.2 dB. MMSE gains will become even larger if more severe (but still realistic) variations are assumed.

The practical value of these first-order minimum-latency adaptation loops is illustrated in Section VII by means of experimental TwoDOS results. In the next section, the minimum-latency adaptation strategy is applied to timing recovery loops.

VI. Minimum-Latency Timing Recovery

For timing recovery, the parameter value θ represents the ideal sampling phase. A second-order loop is generally needed to be able to compensate for frequency errors [21]. In this case, the loop filter $L(f)$ (see Fig. 3) has an integrating path (with gain K_{ti}) to track frequency and a proportional path (with gain K_t) to add a phase correction. The normalized natural frequency of a second-order adaptation loop may be defined as $\omega_n T = \sqrt{K_{ti}}$ and the damping factor as $\zeta = K_t/(2\sqrt{K_{ti}})$ [17]. Besides a loop filter, the timing recovery loop contains a numerically controlled oscillator (NCO) whose phase-domain model is an integrator, and a phase error detector which can be modelled in the phase-domain by a substraction of the estimated phase from the ideal phase.

Ideal sampling phases $\underline{\theta}$ in an experimental 2-D system may be common for all rows (rotation speed variations) but can also be row-dependent [19]. The ideal phase values θ of every row can be written as

$$\theta = \theta_c + \theta_{\mathrm{LF}} = f_p.k + \theta_{\mathrm{HF}} + \theta_{\mathrm{LF}} \tag{11}$$

where θ_c is a component common for all the rows and θ_{LF} is a slowly varying ideal phase component specific for the row under consideration. The common component θ_c has again two terms: a) a frequency deviation term $f_p \cdot k$, where k is the time index and f_p characterizes a small offset between the free-running frequency of the NCO and the frequency of the incoming signal; and b) a common high-frequency phase component θ_{HF}.

Based on this phase-domain parameter model, a minimum-latency strategy can be developed for the timing recovery loop. In Fig. 13, the assumed parameter model together with a parameter-domain model of the minimum-latency timing recovery loops is shown. For simplicity, only two rows are considered: an inner row with small latency and an outer row with large latency. The outer row still has a second-order adaptation loop. A first-order loop filter produces a phase update δ^o which is used as input of the integrator of the outer loop. This phase update δ^o is composed of two components: an estimate of the frequency $\hat{f}_p$ coming from the integrating path (with gain K_{ti}^o) and a phase correction coming from the proportional path (with loop gain K_t^o). Following the minimum-latency adaptation strategy, this phase update δ^o is also used in the inner adaptation loop. In our case, the frequency errors are common across the rows and can be tracked based on the outer rows only. The inner loop is only needed to add a phase correction (accounting for information about θ_{LF}^i) and can therefore remain a first-order loop. Therefore, a zeroth-order loop filter is sufficient (with loop gain K_t^i). Furthermore, a delay of M^i bit intervals is present in the inner loop to mimic the latency introduced by the detector. Input-referred noises ν^i and ν^o are also shown in Fig. 13 and they are assumed to be uncorrelated.

A. Basic Behavior

To understand the basic behavior of the minimum-latency timing recovery loops, the delay M^i of the inner row is omitted ($M^i = 0$) and the input-referred noises ν^i and ν^o are neglected. The behavior of the outer loop is not influenced by the minimum-latency adaptation strategy. As a result, the outer loop has

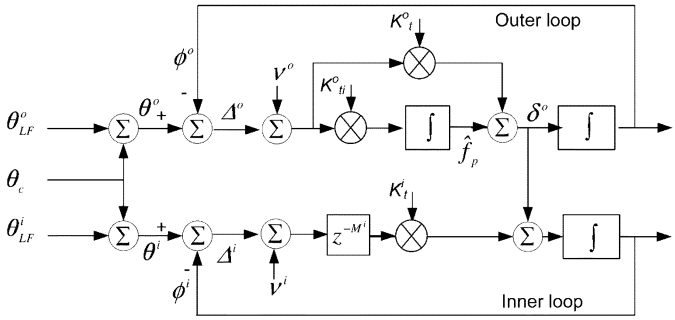

Fig. 13. Parameter-domain model of the minimum-latency timing recovery loops.

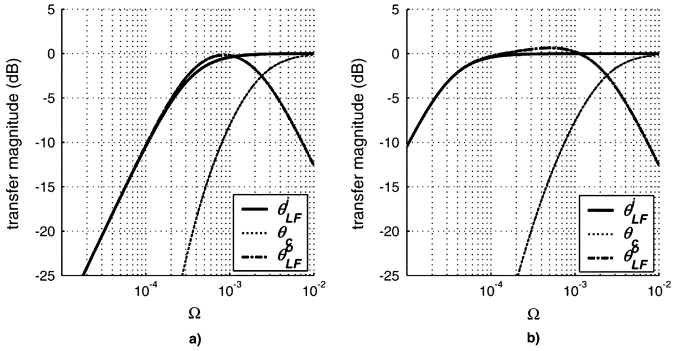

Fig. 14. Mismatch transfer magnitudes of minimum-latency adaptation loops for timing recovery as a function of the normalized frequency $\Omega = \omega T/(2\pi)$. The outer loop is dimensioned with natural frequency $\omega_n^o T = 0.005$ and damping factor $\zeta^o = 1.5$. The inner loop is dimensioned with the following time constants: a) $\tau^i = 500$ bits (left figure). b) $\tau^i = 5000$ bits (right figure).

a second-order behavior. The parameter transfer function of the outer loop is evaluated to be

$$G_{\phi^o}(z) = \frac{\Phi^o(z)}{\Theta^o(z)} = \frac{K_t^o(z-1) + K_{ti}^o}{(z-1)^2}. \tag{12}$$

The parameter transfer function of the inner row is evaluated to be

$$G_{\phi^i}(z) = \frac{\Phi^i(z)}{\Theta^i(z)} = \frac{K_t^i}{z-1}. \tag{13}$$

The z-transform of the inner-loop mismatch Δ^i is evaluated to be

$$\begin{aligned}\Delta^i(z) &= \frac{z-1}{z-1+z^{-M^i}K_t^i}\Theta_{\mathrm{LF}}^i(z) \\ &+ \left(\frac{z-1}{z-1+z^{-M^i}K_t^i}\right)\Theta_c(z) \\ &- \left(\frac{(K_t^o(z-1)+K_{ti}^o)(z-1)}{((z-1)^2+(z-1)K_t^o+K_{ti}^o)\left(z-1+z^{-M^i}K_t^i\right)}\right)\Theta_c(z) \\ &+ \frac{(K_t^o(z-1)+K_{ti}^o)(z-1)}{((z-1)^2+(z-1)K_t^o+K_{ti}^o)\left(z-1+z^{-M^i}K_t^i\right)}\Theta_{\mathrm{LF}}^o(z).\end{aligned} \tag{14}$$

The mismatch transfer magnitudes of the inner loop are shown in Fig. 14.

These magnitudes are similar to the magnitudes for first-order minimum-latency adaptation loops (see Fig. 8). The most important difference is the improved capability of tracking the common component θ_c. For decreasing frequencies, the mismatch magnitude due to the common component θ_c decreases faster with respect to the first-order loops. Moreover, tracking of θ_c is guaranteed up to the outer-row cutoff frequency Ω_c^o, while sufficiently suppressing θ_{LF}^o.

The mismatch Δ^i can be shown to go to zero in case of a frequency step (phase ramp) by observing that

$$\lim_{k\to\infty} \Delta^i[k] = \lim_{z\to 1} \Delta^i(z) = 0 \tag{15}$$

when for $\Delta^i(z)$ we fill in (14), for $\Theta_c(z)$ we apply a phase ramp ($\Theta_c(z) = 1/(z-1)^2$), and for the other inputs we assume zero input ($\Theta_{\mathrm{LF}}^o(z) = 0$ and $\Theta_{\mathrm{LF}}^i(z) = 0$). As a result, no extra measurements have to be taken to guarantee proper convergence of the system.

B. Gradient Noise

The outer-loop gradient noise is not influenced by the inner-loop input-referred noise ν^i. As a result, the variance of the mismatch Δ^o is the same as the variance in a normal second-order loop, and can be expressed as

$$\sigma_{\Delta^o}^2 = \frac{T}{2\pi}\int_{-\frac{\pi}{T}}^{\frac{\pi}{T}} P_{\nu^o}(e^{j\omega T})|G_{\phi^o}(e^{j\omega T})|^2 d\omega. \tag{16}$$

The open-loop transfer function G_{ϕ^o} has an equivalent bandwidth $B_l^o \geq \tilde{B}_l^o = \omega_n^o T(\zeta^o + 1/4\zeta^o)$ (if $\omega_n^o T$ and ζ^o are chosen within the stability range of the second-order loop and the loop-delay M^i is omitted) [17]. Using this normalized equivalent noise bandwidth $\tilde{B}_l^o$, the variance $\sigma_{\Delta^o}^2$ can be written as

$$\sigma_{\Delta^o}^2 = \tilde{B}_l^o \sigma_{\nu^o}^2 \tag{17}$$

if the input-referred noise ν^o is assumed to be white and Gaussian. The gradient noise of the inner loop, however, has an extra component due to the minimum-latency adaptation strategy. The variance of the mismatch Δ^i is evaluated to be

$$\begin{aligned}\sigma_{\Delta^i}^2 = &\frac{T}{2\pi}\int_{-\frac{\pi}{T}}^{\frac{\pi}{T}} P_{\nu^i}(e^{j\omega T})|G_{\phi^i}(e^{j\omega T})|^2 d\omega \\ &+ \frac{T}{2\pi}\int_{-\frac{\pi}{T}}^{\frac{\pi}{T}} P_{\nu^o}(e^{j\omega T})|G_{\phi^o}(e^{j\omega T})|^2 d\omega.\end{aligned} \tag{18}$$

The input-referred noise of the outer loop leaks into the inner loop according to the open-loop transfer function G_{ϕ^o} (with equivalent bandwidth $B_l^o \geq \tilde{B}_l^o = \omega_n^o T(\zeta^o + 1/4\zeta^o)$). Using

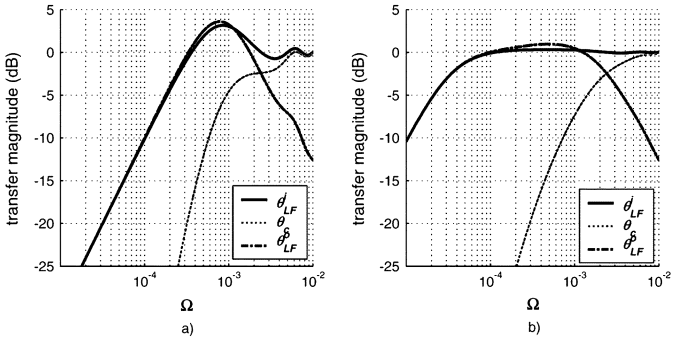

Fig. 15. Mismatch transfer magnitudes of the inner minimum-latency timing recovery loop as a function of the normalized frequency $\Omega = \omega T/(2\pi)$. The inner loop has a loop delay of $M^i = 200$ bits. The outer loop is dimensioned with a natural frequency $\omega_n^o T = 0.005$ and a damping factor $\zeta^o = 1.5$. The inner loop is dimensioned with the following time constants: (a) $\tau^i = 500$ bits (left figure), and (b) $\tau^i = 5000$ bits (right figure).

this normalized equivalent noise bandwidth $\tilde{B}_l^o$, the variance $\sigma_{\Delta^i}^2$ can be written as

$$\sigma_{\Delta^i}^2 \simeq \frac{K_t^i}{2}\sigma_{\nu^i}^2 + \tilde{B}_l^o \sigma_{\nu^o}^2 \simeq \frac{K_t^i}{2}\sigma_{\nu^i}^2 + \sigma_{\Delta^o}^2 \tag{19}$$

if the input noises ν^i and ν^o are assumed to be white and Gaussian. The latter equation indicates that the design of the outer loop (i.e., the choice of values for the natural frequency ω_n^o and the damping factor ζ^o) considerably influences the amount of gradient noise in the inner loop. But $\sigma_{\Delta^i}^2 \approx \sigma_{\Delta^i}^2$ because $K_t^i \ll \tilde{B}_l^o$, i.e., a negligible extra amount of gradient noise is present in the inner timing recovery loop.

C. Behavior of Inner Loop With Latency

Inserting a delay in the inner row of M^i bit intervals causes a degradation in performance of the minimum-latency adaptation loops. The parameter transfer function G_{Φ^i} of the inner row is changed to

$$G_{\Phi^i} = \frac{\Phi^i(z)}{\Theta^i(z)} = \frac{K_t^i z^{M^i}}{z-1}. \tag{20}$$

Consequently also the mismatch of the inner row is changed. In Fig. 15, the mismatch magnitudes due to the different components are shown. A similar reasoning as in Section V-C can be given with the conclusion that the outer loop should be designed slightly faster in order to have MMSE performance.

A resonance peak appears in the transfer magnitudes of the inner loop due to the insertion of the delay M^i. This resonance peak appears near the cutoff frequency Ω_c^i. Consequently, if the second design criterium $(\Omega_c^i > \Omega_{\mathrm{LF}})$ is obeyed, then the overall mismatch power due to the slowly varying component θ_{LF}^i is guaranteed. Furthermore, the outer-row component θ_{LF}^o is rejected sufficiently in the inner-row estimate ϕ^i.

VII. Experimental Results for the TwoDOS System

In the TwoDOS system, bits are stored on a hexagonal lattice [23]. In contrast with conventional optical recording (Compact Disc, CD, Digital Versatile Disc, DVD, and Blu-Ray Disc, BD), where the bits are stored in a single spiral (a one-dimensional sequence of bits), in TwoDOS the bits are organized in a so-called broad spiral. Within a single rotation of this broad spiral, a number N_R of bit rows are stacked upon each other to form a hexagonal structure (see Fig. 16). Adjacent rotations of the broad spiral are separated by a guard band consisting of a bit row without any pits. The data is read out with an array of N_R laser spots arranged such that each spot is centered on one of the bit rows within the broad spiral. A multi-spot photo detector integrated circuit is used to generate a so-called high-frequency (HF) signal for every bit row.

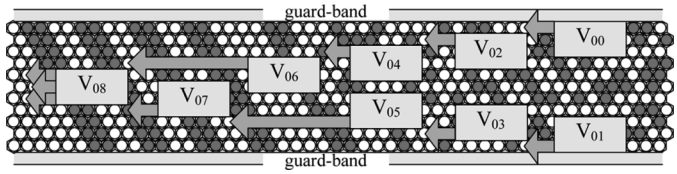

Fig. 16. Example of hexagonal structure for TwoDOS with $N_R = 11$. The configuration of stripe-wise Viterbi detection is also shown for this example: in total 9 stripe detectors $(\mathrm{V}_{00} \ldots \mathrm{V}_{08})$ each covering 3 bit rows are needed to detect the bits of the broad spiral.

A partial response maximum likelihood (PRML) receiver has been built for TwoDOS [19], [24]. It consists of a bit detector preceded by an adaptive equalizer, an adaptive dc compensator, an AGC, and a timing recovery loop. A 2-D Viterbi detector (VD) performs joint bit detection on all bit rows.

To reduce the complexity of a full-fledged 2-D VD, the VD is divided into smaller processing units (called stripe VD). Each stripe VD covers a limited number of bit rows (so-called stripes with a typical height of 2 or 3 bit rows). This detection configuration is called a stripe-wise Viterbi detector (SWVD) [9] and is shown in Fig. 16 together with the hexagonal structure. The stripe VDs (V_{00} up to V_{08} in the figure) are organized in a "V"-shape. The binary output from a first stripe VD is passed to a next stripe VD to be used as side information in the branch metric calculations [9]. As a result, each next stripe VD adds a delay, which is at least equal to the backtracking depth of the stripe VD [19]. As a result, going inwards starting from the outer bit rows the total detection-delay increases considerably. Because all adaptation loops (dc control, AGC, timing recovery, etc.) use the output of the SWVD as side information, the total latency in the loops for the inner rows is large and will limit the tracking capabilities severely.

Laser beam recorded discs with a capacity of 35 GB are placed in an experimental read-out system to produce experimental replay signals. The read-out is conducted under relatively favorable conditions (no scratches, no dropouts, limited amount of dust). Subsequently, the replay signals are digitized and are applied to the TwoDOS receiver in which the minimum-latency adaptation strategy is utilized for dc control and AGC. In this experiment perfect detection is assumed, i.e., the knowledge of the bits written on the disc is utilized in the receiver. Furthermore, the latency M^i induced by the bit detector can be dimensioned freely to monitor the influence of different detection delays on the overall performance of the system.

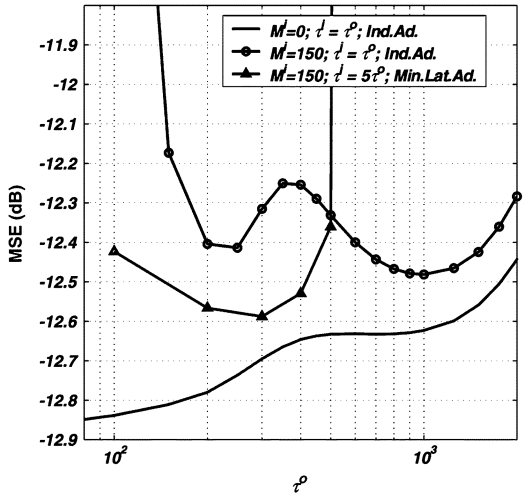

Fig. 17. Inner-row MSE versus τ^o. The time constants of the dc control loop and the AGC loop are taken equal.

The effect of delays on the performance of the first-order dc control loop and the AGC loop is illustrated in Fig. 17. The MSE of the inner row, after convergence of all adaptation loops, is plotted versus the time constant τ^o. The time constants τ^o of the dc control and the AGC loops are taken equal for three different configurations of the adaptation loops: 1) individual adaptation, $M^i = 0$, $\tau^i = \tau^o$; 2) individual adaptation, $M^i = 150$, $\tau^i = \tau^o$; and 3) minimum-latency adaptation, $M^i = 150$, $\tau^i = 5\tau^o$. In this experiment timing recovery is accomplished by individual loops without latency. The natural frequency and damping factor of the second order loops are defined as $\omega_n T = 0.01$ and $\zeta = 1.5$. By analyzing the results shown in Fig. 17, a couple of conclusions can be drawn.

- **Performance of delayed individual adaptation loops:** For small time constants τ^o (fast loops), the performance of the delayed individual adaptation loops is significantly worse with respect to the nondelayed individual loops. The reason for this degradation in MSE is the resonance effect. The spectral content of the system parameter (for the dc-offset in the TwoDOS system, see Fig. 6) near the cutoff frequency Ω_c^i (where also the resonance peak appears) causes a mismatch error increment. For increasing time constants τ^o (i.e., for decreasing capabilities to track rapid variations), the resonance peak decreases and the performance of the delayed experiments rapidly approaches that of the nondelayed experiments. The insertion of a delay in the individual adaptation loops causes a degradation in MMSE of about 0.35 dB.
- **Performance of delayed minimum-latency adaptation loops:** The presence of rapid common variations (see Fig. 6) and the presence of latency in the loops causes an improvement in MSE when going from individual to minimum-latency adaptation loops. The minimum-latency adaptation loops achieve an MMSE improvement of about 0.1 dB with respect to the delayed individual adaptation loops.

To assess the strength of the minimum-latency adaptation strategy, a final experiment was performed: a detection delay is inserted in all inner-row adaptation loops (dc control, AGC and timing recovery), and the minimum-latency adaptation strategy is also applied to all loops. The results are summarized as follows:

Type	MMSE
M = 0, individual adapt.	-12.85
M = 150, individual adapt.	-12.27
M= 150, min.-lat. adapt.	-12.71

The insertion of a delay in the adaptation loops causes a loss of 0.58 dB in MMSE performance for individual adaptation loops. The minimum-latency loops make it possible to approach the optimal nondelayed performance up to 0.14 dB, improving upon individual adaptation by 0.44 dB. By comparing the results of the table and Fig. 17, one can notice that the MMSE obtained for the third case (minimum-latency adaptation and $M = 150$ for all loops) is better than the MMSE in Fig. 17 for the case no latency was present in the timing recovery loop. This MMSE improvement can be explained by the fact that in Fig. 17 the normalized natural frequency and the damping factor of the timing recovery loops were fixed and not optimized, whereas in the table they are optimized to obtain the best performance in the different cases.

The gain in bit error rate is likely to be higher (roughly an order of magnitude for an MSE improvement of 1 dB) but unfortunately insufficient experimental data is available to reliably measure bit error rates [15]. The results obtained in this section were obtained under relatively favorable conditions as ideal parameter values do not have substantial common high-frequency content. As a result, the MMSE gain due to the minimum-latency strategy will be higher if the ideal parameter values will have more common high-frequency content as is the case under extreme situations (severe scratches, dropouts, dust on the disc [20]).

VIII. Conclusion

The presence of delays in adaptation loops introduces resonance effects at frequencies around the cutoff frequency of the loops. These resonance effects cause a degradation of the tracking capabilities of the loop for parameter variations near these frequencies. If these variations are nonnegligible, the performance of the loop can degrade considerably. The performance degradation can be limited through an adaptation strategy in which rapid variations are tracked based on control information from rows with minimum delay. This strategy works well if the rapid parameter variations are common for all the rows. Experimental results for the TwoDOS system show that even under relatively favorable circumstances (without any scratches or dropouts) the MSE gain is already significant (0.44 dB). In practice more extreme situations (scratches, dust, dropouts, etc.) can occur and the gain will then definitely be larger.

Acknowledgment

This work was supported by the European Union under the "TwoDOS" IST Project IST-2001-34168.

REFERENCES

[1] D. M. Bruls, A. H. J. Immink, A. M. van der Lee, W. M. J. Coene, J. Riani, S. Van Beneden, M. Ciacci, J. W. M. Bergmans, and M. Furuki, "Two-dimensional optical storage: High-speed read-out of a 50 GByte single-layer optical disc with a 2D format using $\lambda = 405$ nm and $\mathrm{NA} = 0.85$," in *Int. Symp. Optical Memory*, Jeju, Korea, Oct. 13, 2004.

[2] T. H. M. Akkermans, "Digital control in optical disc drives," in *Int. Conf. Consumer Electronics*, June l9–21, 2001, pp. 246–247.

[3] A. R. Nayak, J. R. Berry, and S. W. McLaughlin, "Optimal placement of training symbols for frequency acquisition: A Cramér-Rao bound approach," *IEEE Trans. Magn.*, vol. 42, no. 6, pp. 1730–1742, Jun. 2006.

[4] W. Zeng, A. Kavcic, and R. Motwani, "Extraction of timing error parameters from readback waveforms," *IEEE Trans. Magn.*, vol. 42, no. 2, pp. 194–199, Feb. 2006.

[5] C. D. Cideciyan, F. Dolivo, R. Hermann, W. Hirt, and W. Schott, "A PRML system for digital magnetic recording," *IEEE J. Sel. Areas Commun.*, vol. 10, no. 1, pp. 38–56, Jan. 1992.

[6] W. M. J. Coene, D. M. Bruls, A. H. J. Immink, A. M. van der Lee, A. P. Hekstra, J. Riani, S. Van Beneden, M. Ciacci, J.W.M. Bergmans, and M. Furuki, "Two-dimensional optical storage," in *IEEE Int. Conf. Acoustics, Speech and Signal Processing*, May 2005.

[7] M. Marrow and J. K. Wolf, "Iterative detection of 2-dimensional ISI channels," in *IEEE Information Theory Workshop 2003*, Mar. 31–Apr. 4, 2003, pp. 131–134.

[8] N. Singla, J. A. O'Sullivan, R. S. Indeck, and Y. Wu, "Iterative decoding and equalization for 2-D recording channels," *IEEE Trans. Magn.*, vol. 38, no. 5, pp. 2328–2330, Sep. 2002.

[9] A. P. Hekstra, W. M. J. Coene, and C. Baggen, "Iterative Stripewise Trellis-Base Symbol Detection Method and Device," Patent Application, no. EP002292937.6; IB2003/005208, Nov. 2003.

[10] L. Huang, G. Mathew, and T. C. Chong, "Reduced complexity Viterbi detection for two-dimensional optical recording," *IEEE Trans. Consumer Electron.*, vol. 51, no. 1, pp. 123–129, Feb. 2005.

[11] M. Marrow and J. K. Wolf, "Detection of 2-dimensional signals in the presence of ISI and noise," in *Int. Symp. Information Theory and its Applications*, Oct. 10–13, 2004, vol. 1, pp. 104–108.

[12] A. P. Hekstra, W. M. J. Coene, and A. H. J. Immink, "Stripe-wise Viterbi detection," *IEEE Trans. Magn.*, submitted for publication.

[13] T. Conway, R. Conway, and S. Tosi, "Signal processing for multitrack digital data storage," *IEEE Trans. Magn.*, vol. 41, no. 4, pp. 1333–1339, Apr. 2005.

[14] Y. Wu, J. A. O'Sullivan, and R. S. Indeck, "Iterative detection and decoding for separable two-dimensional intersymbol interference," *IEEE Trans. Magn.*, vol. 39, no. 4, pp. 2115–2120, Jul. 2003.

[15] A. Immink, "System and receiver design for two-dimensional optical storage," Ph.D. thesis, Univ. Technol. Eindhoven, Eindhoven, The Netherlands, Nov. 2005.

[16] A. M. van der Lee, D. Bruls, C. Busch, A. H. J. Immink, W. M. J. Coene, and A. P. Hekstra, "Two-dimensional optical storage," *Jpn. J. Appl. Phys.*, vol. 43, no. 7B, pp. 4912–914, 2004.

[17] J. W. M. Bergmans, *Digital Baseband Transmission and Recording*. Norwell, MA: Kluwer, 1996.

[18] J. W. M. Bergmans, "Effect of loop delay on stability of discrete-time PLL," *IEEE Trans. Circuits Syst. I, Fundam. Theory Appl.*, vol. 42, no. 4, pp. 229–231, Apr. 1995.

[19] A. H. J. Immink, J. Riani, S. Van Beneden, J. W. M. Bergmans, M. Ciacci, A. N. Irani, W. M. J. Coene, A. M. van der Lee, and D. Bruls, "Adaptation and timing recovery for two-dimensional optical storage," in *Proc. SPIE, ODS*, Apr. 4, 2004.

[20] T. Watanabe, K. Saito, and K. Seo, "Study of error propagation due to dust for thin-cover coat disk systems," in *Int. Symp. Optical Memory and Optical Data Storage Topical Meeting*, Jul. 7–11, 2002, pp. 126–128.

[21] J. Riani, J. W. M. Bergmans, S. Van Beneden, and A. H. J. Immink, "Data-aided timing recovery for recording channels with data-dependent noise," *IEEE Trans. Magn.*, vol. 42, no. 11, pp. 3752–3759, Nov. 2006.

[22] P. F. Odgaard and M. V. Wickerhauser, "Time localisation of surface defects on optical discs," in *Proc. IEEE Int. Conf. Control Applications*, Sep. 2–4, 2004, pp. 111–116.

[23] W. M. J. Coene, "Two-dimensional optical storage," in *ODS 2003, Tech. Dig.*, 2003, pp. 90–92.

[24] T. Conway, "A partial response read channel for two dimensional optical data storage," *IEEE Trans. Consumer Electron.*, vol. 50, no. 4, pp. 1107–1112, Nov. 2004.

Manuscript received April 27, 2005; revised October 18, 2006. Corresponding author: S. Van Beneden (e-mail: s.v.beneden@tue.nl).